

# Tomographic reconstruction of ionospheric electron density based on constrained algebraic reconstruction technique

Debao Wen · Sanzhi Liu · Pingying Tang

Received: 16 November 2009 / Accepted: 29 January 2010 / Published online: 3 March 2010  
© Springer-Verlag 2010

**Abstract** A constrained algebraic reconstruction technique (CART) is proposed for the tomographic reconstruction of the ionospheric electron density distribution. The method uses a popular two-dimensional multi-point finite difference approximation of the second order Laplace operator to provide the constraint matrix. The tomographic results of a numerical simulation show that the reconstruction accuracy of electron density distribution is significantly improved. A careful validation of the reliability and superiority of CART is made. Finally, we applied the new method to the analysis of actual Global Navigation Satellite Systems (GNSS) observations and compared the results with ionosonde observation of Wuhan station.

**Keywords** Ionospheric tomography · TEC · ART · Electron density

## Introduction

Computerized ionospheric tomography (CIT) introduced by Austen et al. (1986) has been become a popular and

successful means for studying the large-scale ionospheric structures over the past decades by using the integrated line-of-sight measurement of polar-orbit satellite observations (Kersley et al. 1993; Foster et al. 1994; Raymund et al. 1994; Kunitsyn et al. 1997; Kunitake et al. 1995; Markkanen et al. 1995; Pryse et al. 1997). Although these studies are useful for understanding the basic ionospheric structures, only a two-dimensional image can be reconstructed since the ground receivers are usually installed along a fixed longitude chain (Wen et al. 2007a; Wen 2010). The present deployment of Global navigation satellite systems (GNSS) receivers, both on ground and onboard satellites, and forthcoming new GNSS satellite constellations are opening a new era for ionosphere imaging by greatly increasing the amount of available data for retrieval of time varying three-dimensional electron density distributions (Garcia and Crespon 2008). In recent years, there have been several reconstructions of the ionospheric electron density distributions based on the GNSS observations (Hansen et al. 1997; Rius et al. 1997; Hernandez-Pajares et al. 1998; Howe et al. 1998; Bust et al. 2000; Liu and Gao 2001; Yin et al. 2004; Jin and park 2007; Wen 2007; Wen et al. 2007b, c, 2008; Andreeva et al. 2009; Lee and Kamalabadi 2009).

Global navigation satellite systems-based CIT requires reconstruction of an image in the region of interest from an ensemble of path integrated projections measured at different angles or along different ray paths. Mathematically, the reconstruction of images from measurements within or around the probing region belongs to the class of so-called inverse problems, in which the required information, such as the distribution of electron density is not directly available. Instead, the available physical parameter is certain measurements of a transformation or a projection of this information. In practice, these measurements are both

D. Wen (✉) · P. Tang  
School of Traffic and Transportation Engineering,  
Changsha University of Science & Technology,  
410004 Changsha, China  
e-mail: iantomography@163.com

D. Wen  
Key Laboratory of Geodynamics,  
Institute of Geodesy and Geophysics,  
Chinese Academy of Sciences, 340 Xudong Road,  
430077 Wuhan, China

S. Liu  
Department of Surveying, Tongji University Shanghai,  
200092 Shanghai, China

an incomplete sampling of information and are corrupted by noise. This makes most inverse problems ill-posed and a direct inversion infeasible. In the process of ionospheric tomographic inversion, the existence of some limitations (e.g., the absence of horizontal ray paths, the limited number of ground stations and finite receiving apertures) often makes the GPS-based ionospheric tomography a subset of an ill-posed problem.

In order to resolve the above problem, numerous algorithms have been presented in recent years. These algorithms can be divided into two categories: iterative reconstruction algorithms and non-iterative reconstruction algorithms. The algebraic reconstruction technique (ART) is a conventional iterative method and simple to compute. It resolves the ill-posed problem by incorporating some prior information into each pixel in an ionospheric tomography system. For those pixels, without any ray paths traversing them, ART algorithm compensates for the incomplete data by using good initial approximations that are usually obtained from empirical ionospheric models such as IRI 2007. This means that the ART is sensitive to the initial approximate. However, the empirical ionospheric models reflect the month-average variation of the ionosphere, so the accuracy of the tomographic results is severely limited. To cope with the limitations, a constrained algebraic reconstruction technique (CART) is presented in this paper. In this new method, the constraint is imposed according to the two-dimensional multi-point finite difference approximation of the second order Laplace operator. A numerical simulation experiment has demonstrated the feasibility of the new method and its superiority to the conventional ART algorithm. Finally, the new method is applied to reconstruct the ionospheric electron density distributions using the regional GPS observation over China, and the advantages of CART are further verified.

## Theory of CIT

In order to reconstruct three-dimensional images of the ionospheric electron density, line integrals of electron density through the probed region must be observed at various positions and orientations. The line integral is the so-called total electron content (TEC), which is written as

$$TEC = \int_l N(l) dl \quad (1)$$

where  $N(l)$  represents the ionospheric electron density and  $l$  specifies the ray path between a satellite and a receiver.

Assuming the electron density distribution to be stable during the selected time period, the imaged region can be

divided into several small pixels. Within each pixel, the electron density is assumed to be a constant, so the continuous density distribution  $N(l)$  is discretized into  $n$  pixels, and the discretized distribution is represented by a column vector  $x$ . The set of TEC measurements is expressed as a column vector  $y$ . In order to relate the discretized electron density distribution to the TEC measurements, a coefficient matrix  $A$  is introduced, so the (1) can be given as

$$y_{n \times 1} = A_{m \times n} x_{n \times 1} \quad (2)$$

The element  $A_{ij}$ , which is the element in the  $i$ th row and  $j$ th column of  $A$ , corresponds to the length of the  $i$ th ray path traversing the  $j$ th pixel.  $m$  represents the number of ray paths, and  $n$  expresses the number of pixels in probed region.

## Constrained ART (CART)

An inversion algorithm is required to determine the unknown electron density distribution from known  $y$  and  $A$ . Many algorithms have been developed to solve (2). ART is very attractive due to its simplicity. The  $k$ th iteration of this algorithm computes the difference between  $y$  and  $y^{(k)}$  where  $y^{(k)}$  is obtained by using the current estimation of  $x^{(k)}$  in (2). A correction derived from this difference is then distributed over  $x^{(k)}$  to obtain  $x^{(k+1)}$ . After much iteration, the result converges to a solution of (2). For the  $k$ th iteration, the algorithm is given by

$$x^{(k+1)} = x^{(k)} + \lambda_k \frac{y_i - \sum_{j=1}^n A_{ij} x_j^{(k)}}{\sum_{j=1}^n A_{ij} A_{ij}} \quad (3)$$

where  $\lambda_k$  is called relaxation parameter; it is the same throughout the iterations. We set the relaxation parameter,  $0 < \lambda_k < 2$ , to 1 for our study. Austen et al. (1986) showed that (3) converges to a solution for expression (1).

Ideally, the number of rays in tomography is larger than the number of pixels, so the ray geometry defines a non-singular matrix, which permits the reconstruction of the probed media. It has been previously mentioned that some limitations make the inversion of electron density rank-deficient. For those pixels without any rays traversing them, the final solution of the ART algorithm is often the same as the corresponding initial value. To cope with this problem, we can introduce additional equations and include them as constraints. These constraints impose smoothness in the solutions. After imposing smoothness, a pixel not hit by any ray will extract the information from its neighbors, while an over-determined pixel will fix its value through the data and contributes to its neighbors' determination. These equations can be written as a new set.

$$B_{l \times n} x_{n \times 1} = 0 \quad (4)$$

where  $B$  is the horizontal constraint matrix and  $l$  is the number of constraint equations.

Proper selection of the deterministic  $B$  in (4) is crucial to the tomographic reconstruction of ionospheric electron density distribution. One way to do this is to use the two-dimensional multi-point finite difference approximation of the second order Laplace operator. Figure 1 illustrates the discretization of the media in one plane.

According to the basic constraint rules, for those pixels that lie at the center of the probed region, the constraint is given by using the following two-dimensional nine-point finite difference approximation of the second order Laplace operator (Hobiger et al. 2008).

$$L_0 = \begin{bmatrix} -1 & -1 & -1 \\ -1 & 8 & -1 \\ -1 & -1 & -1 \end{bmatrix}$$

The operator has to be adjusted accordingly when the pixels locate at the edge of the probed region. For those pixels lying on the four corners of one layer, the operators are given in  $L_1$  (the lower-left pixel),  $L_2$  (the lower-right pixel),  $L_3$  (the top-left pixel) and  $L_4$  (the top-right pixel).

$$L_1 = \begin{bmatrix} -1 & -1 \\ 3 & -1 \end{bmatrix} \quad L_2 = \begin{bmatrix} -1 & -1 \\ -1 & 3 \end{bmatrix} \quad L_3 = \begin{bmatrix} 3 & -1 \\ -1 & -1 \end{bmatrix} \quad L_4 = \begin{bmatrix} -1 & 3 \\ -1 & -1 \end{bmatrix}$$

However, for those pixels lying on the edge rather than the corner, the operators are given in  $L_5$  (the pixels of lower boundary),  $L_6$  (the pixels of top boundary),  $L_7$  (the pixels of left boundary) and  $L_8$  (the pixels of right boundary).

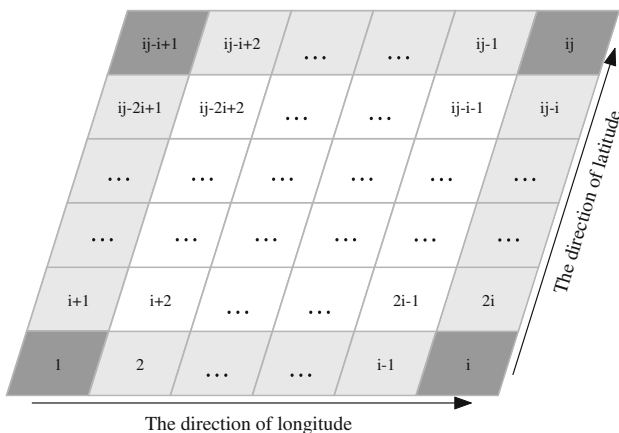


**Fig. 1** Sketch of the discretization for one layer

$$L_5 = \begin{bmatrix} -1 & -1 & -1 \\ -1 & 5 & -1 \\ -1 & -1 & -1 \end{bmatrix} \quad L_6 = \begin{bmatrix} -1 & 5 & -1 \\ -1 & -1 & -1 \\ -1 & -1 & -1 \end{bmatrix} \quad L_7 = \begin{bmatrix} -1 & -1 \\ 5 & -1 \\ -1 & -1 \end{bmatrix} \quad L_8 = \begin{bmatrix} -1 & -1 \\ -1 & 5 \\ -1 & -1 \end{bmatrix}$$

As for other layers, the operators are given by using the earlier rules. According to the operators, the constrained matrix  $B$  in (4) can be created.

### Test case using artificial data

A simple test case is devised to validate the performance of the CART algorithm in comparison with the ART algorithm that has been widely applied to ionospheric tomography. In the test, the electron density distribution is generated by using the international reference ionosphere (IRI) model. IRI 2007 is applied in this research. The reconstructed range in latitude is selected from 30 to 36°N for 05:30–06:00UT, November 20, 2008. The longitude ranged from 116 to 122°E, and the height ranged from 100 to 700 km in steps of 10 km. The discretized interval in latitude and longitude is 0.5 and 1°, respectively. For the test of CART, the actual positions of the GPS satellites and the ground receivers during the selected time period are used to create the matrix  $A$ . In order to evaluate the error of the analysis, the average density error  $E_d$  is defined as

$$E_d = \frac{\sum_{j=1}^n \tilde{x}_j - x_j}{n} \quad (5)$$

where  $x$  and  $\tilde{x}$  are the original (IRI 2007) and the reconstructed density distributions, respectively.

Model observation data, corresponding to 05:30–06:00UT, November 20, 2008, for 44 GPS receivers located in Jiangsu province in China, were produced to test our reconstruction method. Then, the electron density distribution is reconstructed by using both CART algorithm and ART algorithms. The comparisons between the electron density distributions obtained from the IRI 2007 model and those reconstructed from two algorithms are shown in Fig. 2. From Fig. 2, we can see that the reconstructed result of the CART algorithm agrees better than that of the ART algorithm. The recovered electron density distribution looked very similar to that given by IRI 2007 model, and the density values were modified with the information from the neighboring ones by the Laplacian constraint as expected. In the reconstructed results of the CART algorithm, the maximum of the absolute errors is  $3.2 \times 10^{10}$  el/m<sup>3</sup>, the average density error  $E_d$  is  $8.2 \times 10^9$  el/m<sup>3</sup>, which is very small compared with the typical peak density of  $1.03 \times 10^{12}$  el/m<sup>3</sup>. However, in the reconstructed results of the ART algorithm, the maximum

**Fig. 2** Comparison between the electron density distribution of the model data (*broken line*) and the corresponding distribution of the electron density reconstructed by the two algorithms (*solid line*) **a** CART; **b** ART. The unit of ionospheric electron density is  $10^{11}$  el/m $^3$

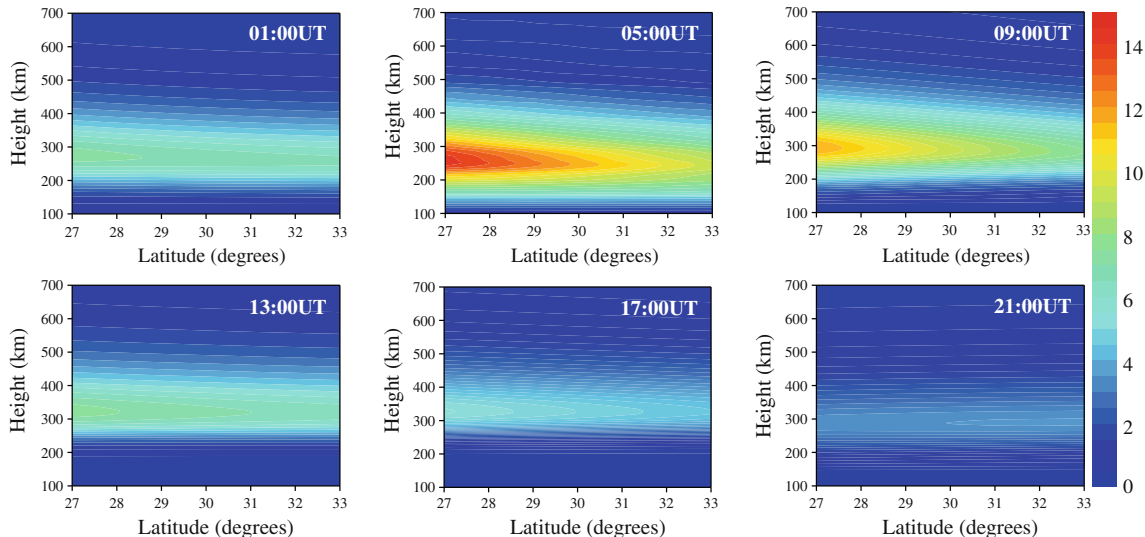
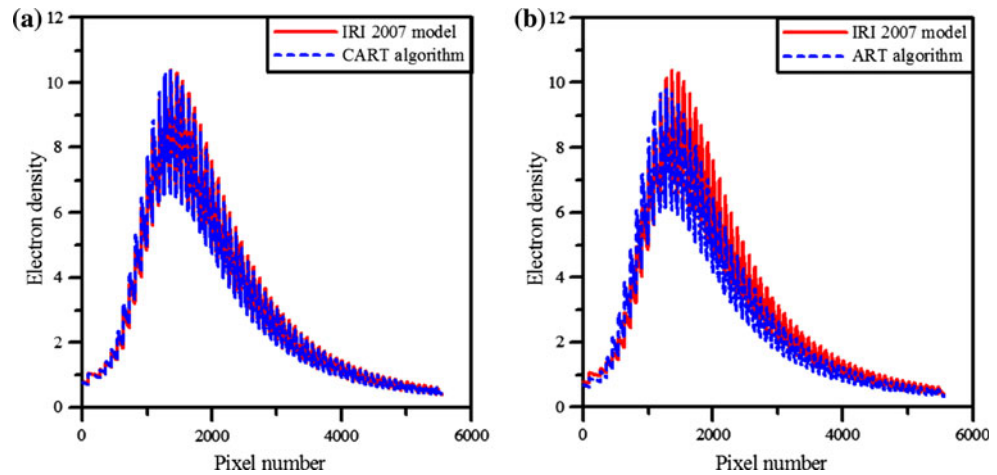


**Fig. 3** Sample of ionospheric electron density distribution obtained from August 17, 2003. Each *snapshot* represents the corresponding electron density reconstructed at different universal time, which is

labeled at the *right-top corner* of the *snapshot*. The unit of electron density is  $10^{11}$  el/m $^3$

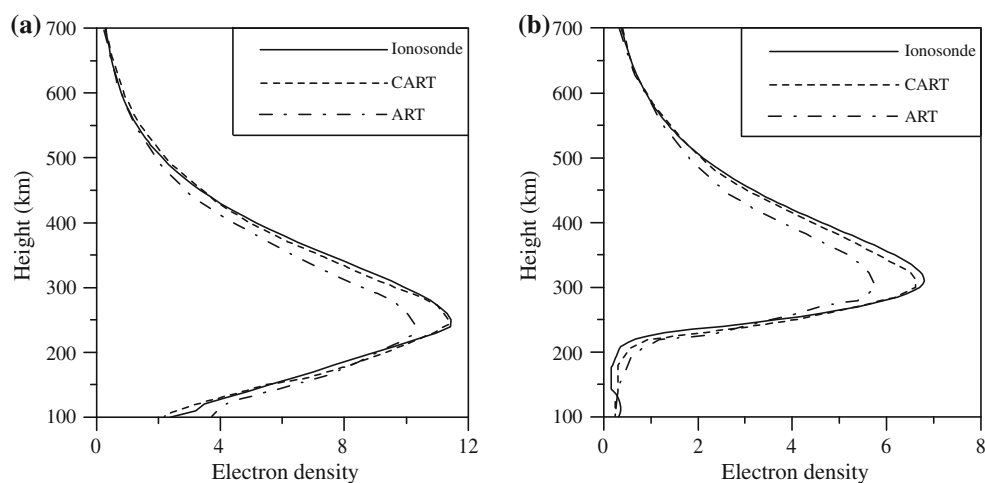
of the absolute errors is  $1.15 \times 10^{11}$  el/m $^3$ , the average density error  $E_d$  is  $3.7 \times 10^{10}$  el/m $^3$ . The statistics of the reconstructed error validates that the CART algorithm is superior to the ART algorithm.

### Reconstruction of the electron density distribution from actual GPS observation data

For additional testing of the characteristic of CART, we apply the new algorithm to actual GPS observation data obtained from 23 different receivers. Observation data within 30 min every hour are used to study the effects of

diurnal variations in the ionosphere. Figure 3 shows some examples of typical tomographic images of the ionosphere during the magnetically quiet period on August 17, 2003. A height-versus-geographic latitude grid has been used. It can be seen from Fig. 3 that the ionospheric electron density varies from small to large value and then from large to small value with the earth's rotation from west to east. Meanwhile, Fig. 3 shows that the value of ionospheric electron density in the north is generally smaller than that in the south. It reflects the existence of a close relationship between the variations of ionosphere with the latitude. Figure 3 also shows that the peak height of the ionosphere first rises and then it falls.

**Fig. 4** Comparisons between the vertical electron density distribution obtained from ionosonde data and the corresponding density distributions reconstructed by the CART and ART algorithms at 05:00UT and 13:00UT. **a** 09:00UT; **b** 13:00UT. The unit of electron density is  $10^{11}$  el/m<sup>3</sup>



The ionosonde station (Wuhan) in China provided an independent comparison with the tomographically reconstructed electron density profiles from the CART and ART algorithms. Figure 4 gives the comparisons at 05:00UT and 13:00UT. It can be seen from Fig. 4 that the tomographically reconstructed profiles of CART algorithm have a better agreement with ionosonde data from Wuhan station than those reconstructed from ART algorithm as a whole. The comparisons further verify the reliability of CART and its superiority to the ART when the actual GPS observations are used.

## Discussions and conclusions

A new reconstruction algorithm of electron density distribution, called the CART, has been presented in this work. The CART algorithm imposes a constraint according to the smoothness of neighboring pixels. It overcomes to some extent the disadvantages of the ART algorithm. The CART algorithm was applied to the reconstruction of the ionospheric electron density distribution from TEC. The feasibility of this new method was validated by numerical simulations in which reasonable density distributions were reconstructed from TEC generated from IRI 2007 model. The simulations showed that the new method is superior to the conventional ART. After careful examination of the results of these simulations, the CART algorithm was applied to the reconstruction of TEC observed in a magnetically quiet period, and the large-scale structure of the ionosphere was reconstructed. The profile reconstructed from CART has a better agreement with ionosonde than that from ART. This paper shows that the CART algorithm is effective in ionospheric tomography.

Although the CART algorithm has been applied to three-dimensional ionospheric tomography, it is not limited to this single application. It can also be used in other kind of tomography inversions as long as constraints can be defined in a meaningful sense. This method is expected to extend to four-dimensional tomography in the future by considering temporal evolution of the ionosphere.

**Acknowledgments** This research is supported by the National Natural Science Foundation of China (Grant No. 40804002), the National Science Fund for Distinguished Young Scholars of China (Grant No. 40625013) and the Scientific Research Fund of Hunan Provincial Education Department (09B007). The authors would also like to thank the anonymous reviewers for their constructive suggestions toward the improvement of this paper.

## References

- Andreeva ES, Kunitsyn VE, Leonyeva EA (2009) The ionosphere over Alaska during a storm period in October 2003: radio tomography and data obtained with GAIM/IFM ionospheric models. *Moscow University Phys Bull* 64(1):84–88
- Austen JR, Franke SJ, Liu CH (1986) Applications of computerized tomography techniques to ionospheric research. In: Tauriainen A (Ed) *Radio beacon contribution to the study of ionization and dynamics of the ionosphere and corrections to geodesy*. Oulu part 1: pp. 25–32
- Bust GS, Coco D, Makela JJ (2000) Combined ionospheric campaign 1: ionospheric tomography and GPS total electron content (TEC) depletions. *Geophys Res Lett* 27(18):2849–2852
- Foster JC, Buonsanto MJ, Holl MJ (1994) Russian-American tomography experiment. *Int J Imaging Sys Tech* 5:148–159
- Garcia R, Crespon F (2008) Radio tomography of the ionosphere: Analysis of an underdetermined, ill-posed inverse problem, and regional application. *Radio Sci* 43: RS2014. doi:[10.1029/2007RS003714](https://doi.org/10.1029/2007RS003714)
- Hansen AJ, Walter T, Enge P (1997) Ionospheric correction using tomography. In: Proceedings of Institute of Navigation ION GPS-97, Kansas City, pp 249–260

- Hernandez-Pajares M, Juan JM, Sanz J (1998) Global observation of the ionosphere electronic response to solar events using ground and LEO GPS data. *J Geophys Res* 103(A9):20789–20796
- Hobiger T, Kondo T, Koyama Y (2008) Constrained simultaneous algebraic reconstruction technique (C-SART)—a new and simple algorithm applied to ionospheric tomography. *Earth Planets Space* 60:727–735
- Howe BM, Runciman K, Secan JA (1998) Tomography of Ionosphere: four-dimensional simulations. *Radio Sci* 33(1):109–128
- Jin SG, Park JU (2007) A comparison with the IRI-2001 model over South Korea. *Earth Planets Space* 59:287–292
- Kersley L, Heaton JAT, Pryse SE (1993) Experimental ionospheric tomography with ionosonde input and EISCAT verification. *Ann Geophys* 11(11–12):1064–1074
- Kunitake M, Ohtake K, Maruyama T (1995) Tomographic imaging of the ionosphere by the modified truncated SVD method. *Ann Geophys* 13:1303–1310
- Kunitsyn VE, Andreeva ES, Razinkov OG (1997) Possibilities of the near-space environment radiotomography. *Radio Sci* 32(5):1953–1963
- Lee JK, Kamalabadi F (2009) GPS-based radio tomography with edge-preserving regularization. *IEEE Trans Geosci Remote Sensing* 47(1):312–324
- Liu ZZ, Gao Y (2001) Optimization of Parameterization in ionospheric tomography. In: Proceedings of Institute of Navigation GPS 2001, Salt Lake City, pp 2277–2285
- Markkanen M, Lehtinen M, Nygren T, Pirttilä J, Henelius P, Vilenius E, Tereshchenko ED, Lhuduk BZ (1995) Bayesian approach to satellite radio tomography with applications in the Scandinavian sector. *Ann Geophys* 13:1277–1287
- Pryse SE, Kersley L, Williams MJ (1997) Tomographic imaging of the polar-cap ionosphere over Svalbard. *J Atmos Terr Phys* 59:1953–1959
- Raymund TD, Austen JR, Franke SJ (1994) Ionospheric tomography: its limitations and reconstruction methods. *J Atmos Terr Phys* 56(5):637–657
- Rius A, Ruffini G, Cucurull L (1997) Improving the vertical resolution of ionospheric tomography with GPS occultations. *Geophys Res Lett* 14(18):2291–2294
- Wen DB (2007) Imaging the ionospheric electron density using a combined tomographic algorithm. In: Proceedings of Institute of Navigation GNSS 2007, Fort Worth City, pp 2337–2345
- Wen DB (2010) The research development of computerized ionospheric tomography technique. *Bull Nat Sci Foun China* 24(1):17–20
- Wen DB, Yuan YB, Ou JK (2007a) Monitoring the three-dimensional ionospheric electron density distribution using GPS observations over China. *J Earth Syst Sci* 116(3):235–244
- Wen DB, Yuan YB, Ou JK (2007b) Ionospheric temporal and spatial variations during the 18 August 2003 storm over China. *Earth Planets Space* 59:313–317
- Wen DB, Yuan YB, Ou JK, Zhang KF (2007c) Three dimensional ionospheric tomography by an improved algebraic reconstruction technique. *GPS Solut* 11(4):251–258
- Wen DB, Yuan YB, Ou JK (2008) A hybrid reconstruction algorithm for three dimensional ionospheric tomography. *IEEE Trans Geosci Remote Sensing* 46(6):1733–1739
- Yin P, Mitchell CN, Spencer PSJ (2004) Ionospheric electron concentration imaging using GPS over the USA during the storm of July 2000. *Geophys Res Lett* 31:L12806. doi:[10.1029/2004GL019899](https://doi.org/10.1029/2004GL019899)

## Author Biographies



**Debao Wen** received the B.Sc. degree in surveying engineering from Henan Polytechnic University, Jiaozuo, China and the Ph.D. degree in geodesy and surveying engineering in 2008 from the Chinese Academy of Sciences (CAS) Wuhan. He is currently with the Changsha University of Science and Technology, Changsha, China and with the Institute of Geodesy and Geophysics, CAS. His current research projects include three-dimensional ionospheric/atmospheric tomography based on GNSS observations and the effects of space weather on navigation and positioning. Dr. Wen has received several awards, including the Prize of Chinese Military Science and Technology Advance, Excellent Prize of the Presidential Scholarship of CAS, Best Paper of ION GNSS 2007.



**Sanzhi Liu** received the B.Sc. and M.Sc. degrees in surveying from Henan Polytechnic University, China. She is currently working towards the Ph.D. degree in surveying at the Tongji University, Shanghai. She is a lecturer with Nanjing University of Technology, China. Her research interest includes study of signal propagation through the ionosphere.



**Pingying Tang** received the B.Sc. degree in Engineering of Surveying and Mapping from Central South University, China and the M.Sc. degree in Road Engineering in 1996 from Hunan University, China. She is currently working towards the Ph.D. degree in Engineering of Surveying and Mapping at the Central South University, Changsha. She is an associate professor with Changsha University of Science and Technology, China. Her research interest includes study of crustal deformation measurement and the application of GPS.